Environmental Science & Technology

Article

pubs.acs.org/est

Tellurium Distribution and Speciation in Contaminated Soils from Abandoned Mine Tailings: Comparison with Selenium

Hai-Bo Qin,*[,†,‡] Yasuo Takeichi,[§] Hiroaki Nitani,[§] Yasuko Terada,[∥] and Yoshio Takahashi*[,‡]

[†]State Key Laboratory of Environmental Geochemistry, Institute of Geochemistry, Chinese Academy of Sciences, Guiyang 550081, China

[‡]Department of Earth and Planetary Science, Graduate School of Science, The University of Tokyo, Hongo 7-3-1, Bunkyo-ku, Tokyo 113-0033, Japan

[§]Institute of Materials Structure Science, High Energy Accelerator Research Organization (KEK), 1-1 Oho, Tsukuba, Ibaraki 305-0801, Japan

[∥]Japan Synchrotron Radiation Research Institute (JASRI), SPring-8, 1-1-1 Kouto, Sayo-cho, Sayo-gun, Hyogo 679-5148, Japan

Supporting Information

ABSTRACT: The distribution and chemical species of tellurium (Te) in contaminated soil were determined by a combination of microfocused X-ray fluorescence (μ-XRF), X-ray diffraction (μ-XRD), and X-ray absorption fine structure (μ-XAFS) techniques. Results showed that Te was present as a mixture of Te(VI) and Te(IV) species, while selenium (Se) was predominantly present in the form of Se(IV) in the soil contaminated by abandoned mine tailings. In the contaminated soil, Fe(III) hydroxides were the host phases for Se(IV), Te(IV), and Te(VI), but Te(IV) could be also retained by illite. The difference in speciation and solubility of Se and Te in soil can result from different structures of surface complexes for Se and Te onto Fe(III) hydroxides. Furthermore, our results suggest that the retention of Te(IV) in soil could be relatively weaker than that of Te(VI) due to structural incorporation of Te(VI) into Fe(III) hydroxides. These findings are of geochemical and environmental significance for better understanding the solubility, mobility, and bioavailability of Te in the surface environment. To the best of our knowledge, this is the first study reporting the speciation and host phases of Te in field soil by the μ-XRF–XRD–XAFS techniques.

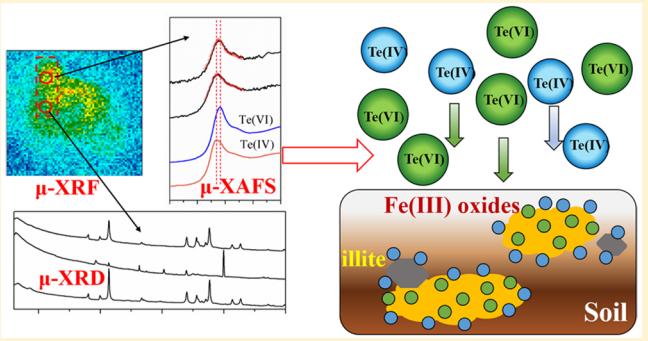

INTRODUCTION

Tellurium (Te) has attracted increasing attention due to its wide industrial applications, such as improving optoelectronic and thermal properties of steel and glass and developing new materials (e.g., CdTe thin-film solar panels) as well as producing fluorescent probes.[1−4] As expected, the expanded use of Te can lead to environmental pollution and induce acute and chronic Te poisoning to human (e.g., the degeneracy of liver and kidney).[2,5] The Occupational Safety and Health Administration (OSHA) has set the permissible exposure limit for workers to Te compounds in the workplace as 0.1 mg m^{-3} over an 8 h workday.[5] In addition, radiotellurium including ^{127m}Te, ^{129m}Te, ^{131m}Te, and ^{132}Te may be released into the environment in the case of the nuclear accidents (e.g., the Fukushima Daiichi Nuclear Power Plant accident in March 2011), which are severely harmful to human health through the inhalation and ingestion of contaminated crops.[6,7]

Tellurium is one of the least-abundant elements in the earth's crust, but it is considerably enriched in marine ferromanganese crusts.[1,8,9] The environmental fates and biogeochemical behaviors of Te are still poorly known, although its chemical and physical properties are generally considered to be similar to those of selenium (Se) in the same Group 16 of the periodic table. It was recently suggested that the distribution behavior between Te and Se is significantly different in a laboratory soil–water system,[10] but similar studies in natural systems are lacking due to extremely low Te concentration in geological, environmental, and biological samples.

In the natural environment, Te occurs in several oxidation states (−II, 0, IV, and VI) and organic forms.[1,2] Oxyanion tellurate (Te(VI)) is the predominant species of Te in hydrosphere.[9,11] Tellurite (Te(IV)) is another soluble form, but its toxicity is 10-fold higher than that of Te(VI).[12] Te(IV) is toxic to bacteria even at a low concentration, yet some Te-resistant bacteria that can reduce Te(IV) and Te(VI) to elemental Te(0) have been found in nature.[13−15] Elemental Te(0) is insoluble in water and, thus, has less mobility and

Received: February 20, 2017
Revised: April 19, 2017
Accepted: April 20, 2017
Published: April 20, 2017

DOI: 10.1021/acs.est.7b00955
Environ. Sci. Technol. 2017, 51, 6027−6035

toxicity. These microorganisms could be used to relieve excessive Te in aquatic environment via microbial reduction from Te oxyanions to precipitated Te(0).[14,15] Various telluride minerals such as calaverite ($AuTe_2$), rickardite (Cu_7Te_5), and sylvanite (Ag_3AuTe_2) often coexist in gold (Au) deposits,[1,16] while organic forms of Te (e.g., dimethyl telluride, telluro-cystine, and telluro-methionine) are mainly related to biological activities.[1,2] Thus, Te speciation is crucial for better understanding its distribution, bioavailability, toxicity, and mobility in the environment because different forms show the unique biogeochemical properties.

However, research regarding the distribution and chemical speciation of Te in field soil has been scarcely attempted, owing to challenging analytical methods for Te speciation.[17] In the past few decades, the X-ray absorption fine structure (XAFS) method, which consists of X-ray absorption near edge structure (XANES) and extended X-ray absorption fine structure (EXAFS) spectroscopy, has been widely utilized to non-destructively identify metal(loid)s speciation in solid samples.[10,18−21] Nevertheless, Te speciation in common soil containing low Te content could not be determined by XAFS technique with reasonably high detection limit. Furthermore, the absorption energies of the K-edge and L_{III}-edge of Te are 31814 and 4341 eV, respectively, but both energies are inaccessible at many traditional XAFS beamlines in the world. The consequence is that synchrotron-based XAFS measurement is difficult to be carried out even if Te content in the solid sample is high enough to collect the XAFS spectra of Te.

The Kawazu Mine located at Shimoda City, Shizuoka Prefecture, Japan, is famous for the occurrence of Au−Ag−Te−Mn veins, where a unique Te mineral named kawazulite (Bi_2Te_2Se) has been discovered.[22−24] However, Te level and speciation in the soil around Kawazu Mine are largely unknown. In this study, we have investigated Te concentration in the soils from abandoned Kawazu Mine tailings. Furthermore, the chemical speciation and host phases of Te in the contaminated soil have been identified using powerful micro focused XAFS (μ-XAFS), X-ray fluorescence (μ-XRF), and X-ray diffraction (μ-XRD) techniques. The aims of this study were (i) to clarify the distribution and speciation of Te in the contaminated soil and (ii) to further provide valuable insights into the migration, bioavailability, and potential risk assessment of Te in the surface environment.

MATERIALS AND METHODS

Sample Collection and Preparation. The soil samples were collected around Hinokizawa pithead (34.41° N, 138.55° E) of Kawazu Mine (Figure S1), and details on its geology and ore deposit are given in the Supporting Information. In the laboratory, soil samples, free of plant roots and detritus, were air-dried and then ground with an agate mortar for chemical and speciation analysis. Furthermore, a thin section of the soil sample that has been first sieved to eliminate large particles (<0.5 mm) was prepared for the μ-XRF−XRD−XAFS measurements (details are given in the Supporting Information). The determination of total Te concentration in sample is described in the Supporting Information.

***μ*-XRF and *μ*-XAFS Measurement.** The μ-XRF mapping and Te K-edge μ-XAFS experiments for the soil sample were performed at BL37XU, SPring-8 (Hyogo, Japan). The incident beam was monochromatized at 35 keV with a Si(111) double-crystal monochromator and then focused to 0.9 μm (V) × 1.3 μm (H) with a rectangular form at the sample position by a Kirkpatrick−Baez (K−B) mirror system. The sample was mounted on a XY sample stage oriented at 10° to the orthogonal direction of the beam, and the fluorescence X-rays from sample was monitored by a Ge solid-state detector (SSD) placed at 90° to the incident X-ray beam.

To realistically reflect the distribution and speciation of Te in soil, five scan areas were randomly selected in the soil thin-section sample. More than 20−50 soil particles were surveyed in each scan area. In the scan, large aggregates were not examined (note that most of large particles have been already removed by sieving) because the aggregate usually containing complex and mixed minerals makes it difficult to accurately identify the host phases of Te in soil. The μ-XRF maps of soil grains for elements including Te, iron (Fe), and Se were obtained by mapping at a pixel size of 3 μm × 3 μm and a dwell time of 0.2 s under ambient conditions.

Based on the μ-XRF maps of Te, hot-spots in soil with higher Te intensity were selected to collect μ-XAFS spectra in fluorescence mode through moving XY sample stage controlled by pulse motors. The fluorescence intensity was recorded by the Ge SSD (SEIKO EG&G), whereas the reference compounds (e.g., Na_2TeO_3 and $Na_2H_4TeO_6$) were analyzed in transmission mode. Energy calibration was performed using a reference compound of Na_2TeO_3 by defining the energy of 31811 eV at the maximum peak of the Te K-edge.

***μ*-XRD Measurement.** The μ-XRD measurement was conducted at beamline BL-15A1, Photon Factory (Tsukuba, Japan), which was recently developed to be capable of simultaneous XRF-XRD-XAFS mapping.[25] The mirror optics of the beamline provides an intense X-ray beam of ~10^{11} photons/sec with an X-ray beam ~20 μm in diameter. This station is equipped with an ion chamber for transmission XAFS, a silicon-drift detector (SDD) for XRF, and a two-dimensional pixel array detector (PILATUS 100 k) for XRD measurements. The sample surface can be monitored using an online optical microscope, and the sample position is scanned with a motorized linear stage. The angles of sample and XRD detector can be altered with a goniometer to avoid diffraction X-ray deteriorating XRF signals and to collect appropriate XRD patterns. In this study, the spots in soil grains where μ-XAFS spectra were collected at BL37XU (SPring-8) were selected to carry out XRD measurement for identifying dominant minerals. Moreover, the μ-XRD patterns for some hot-spots in the soil sample were also measured at beamline 10.3.2 at the Advanced Light Source (ALS) in the Lawrence Berkeley National Laboratory (see the Supporting Information).

XAFS Data Analysis. The XAFS data were analyzed using REX2000 (Rigaku Co. Ltd.) and FEFF 7.02 code.[26] Quantitative analysis of XANES was performed by linear combination fitting (LCF) using $Na_2H_4TeO_6$ and Na_2TeO_3 as end members in the range of 31800−31835 eV. For EXAFS analysis, the radial structure function (RSF) was obtained through extracting EXAFS oscillation and Fourier transformation (FT). The distinct shells of the RSFs were then back-transformed to k-space for spectral simulation by curve-fitting analysis. The backscattering amplitudes and phase shifts for fitting were extracted from model compounds such as Fe_2TeO_5[27] and Fe_2TeO_6.[28] The quality of XANES and EXAFS simulation were evaluated by the goodness of fit parameter (R factor), and further details are given in the Supporting Information.

Adsorption Experiments. The adsorption experiments of Te on ferrihydrite, goethite, and illite (IMt-1, Silver Hill, MT)

DOI: 10.1021/acs.est.7b00955
Environ. Sci. Technol. 2017, 51, 6027−6035

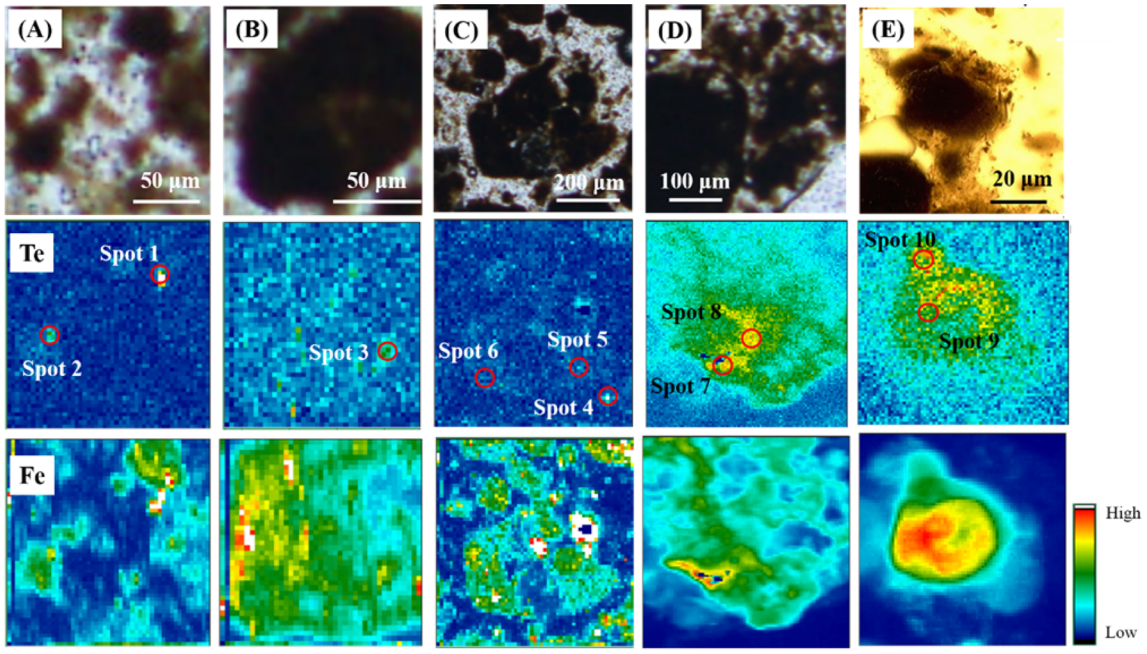

Figure 1. μ-XRF maps of selected areas in contaminated soil. The upper figures are optical image of five interested areas (A–E), while the middle and lower figures show the maps of Te and Fe, respectively. The open circles in Te maps indicate interested hot-spots for further μ-XAFS measurement.

were conducted in polystyrene vessels under ambient conditions using the batch approach. Moreover, further EXAFS analyses were conducted for some solid phases used as model compounds through filtering the final suspension of iron oxides. Details concerning the synthesis of two-line ferrihydrite and goethite, adsorption experiments, and bulk EXAFS measurement for adsorbed samples are described in the Supporting Information.

RESULTS AND DISCUSSION

Tellurium Contamination in Soils from Abandoned Mine Tailings. The average of the total Te concentration in soils from abandoned tailings in Kawazu Mine was 15.2 ± 2.7 mg kg^{-1} (n = 9), with a range from 10.2 to 18.0 mg kg^{-1} (Table S1 and Figure S2). This value is approximately 203, 507, and 563 times greater than average Te content in soils collected in Japan (0.075 mg kg^{-1}),[7] Europe (0.03 mg kg^{-1}),[29] and worldwide (0.027 mg kg^{-1}),[2] respectively. In comparison with soils contaminated by the metal refinery,[30] Te levels in soils from the study area are also considerably higher than the reported values (0.02–11.1 mg kg^{-1}). These facts indicate that the soils surrounding Hinokisawa pithead of Kawazu Mine have been heavily contaminated by Te.

A significant decrease in the total Te concentration was observed in soils with the distance from mining tailings (Figure S2). Te content in one soil sample with a distance of about 100 m away from pithead (0.12 mg kg^{-1}) was much lower compared with contaminated soils (10.2–18.0 mg kg^{-1}) but is within the range of Te levels in agricultural soils from Japan (0.015–0.85 mg kg^{-1}).[7] This suggests that Te contamination in soil is probably dependent on the effect of abandoned tailings, but the migration of Te in surface environment seems to be poor.

The Kawazu Mine was mainly exploited for gold and silver, and thus, most of Te can be still preserved in the waste tailings during mining process. Although Te occurs as the primary form of native Te and telluride minerals in the Au–Ag-bearing veins at Hinokizawa Mine,[22−24] these primary Te minerals could be transformed to secondary Te oxyanions of tellurite and tellurate under appropriate conditions. In particular, pyrite, a dominant sulfide in the Te-bearing microbands, can accelerate this transformation of Te speciation through creating a low-pH environment during its weathering processes under oxic conditions. As a consequence, these soluble oxyanions, i.e., Te(IV) and Te(VI), which are transformed from Te minerals in tailings, can be retained by soil particles and accumulated in the soils around abandoned mine tailings at Hinokizawa area.

The metal(loid)s contamination in soil can be caused by geogenic (e.g., underlying bedrock and groundwater) and anthropogenic (e.g., mining, refining, and fertilization) factors. For contaminated soils from the study area, the geogenic contribution should be very small considering that Te concentration in the soil far away from the tailings was ~100-fold lower than that in contaminated soil. Additionally, it has been documented that metal processing in the early period of nickel refinery can have led to elevated Te content in the surrounding topsoil.[30] However, there were no refineries in the vicinity of Kawazu Mine in history. Thus, it is reasonable to conclude that Te in soils surrounding Kawazu Mine is mainly derived from abandoned mine tailings, and Te contamination in soil has remained even after the cessation of the mining activities since 1959.

X-ray Spectroscopy Analyses for Contaminated Soil. *μ-XRF Analyses.* The nonuniform distribution for Te were observed in the soil thin section by the μ-XRF mapping (Figure 1), suggesting that Te in contaminated soil is highly heterogeneously distributed. Elevated intensity of Te was generally found in the soil particles with higher intensity of Fe, which implies that Fe-containing minerals are likely to be the host phases of Te. This is consistent with the observation that Fe (oxyhydr)oxide can be the host phases of Te in ferromanganese crust[18] and incubated soils under oxic

DOI: 10.1021/acs.est.7b00955
Environ. Sci. Technol. 2017, 51, 6027–6035

conditions.[10] Nonetheless, Te hot-spots were not strictly observed in the Fe-rich grains in the soil thin section, and not all Fe hot-spots contain more Te. This distribution discrepancy of Te and Fe in soil might be caused by their different probing depths because higher energy of Te (Kα: 27.382 keV) can result in a deeper escape depth relative to that of Fe (Kβ: 7.058 keV). However, the highest possibility is that Te can also be associated with other phases in soil in addition to Fe oxides.

μ-XRD Analyses. The μ-XRD patterns for Te hot-spots are shown in Figure S3. It was observed that μ-XRD patterns for the same hot-spot (e.g., spot 8) collected at beamline 10.3.2 at the ALS or BL-15A1 at Photon Factory were highly comparable, indicating that both beamlines can be used to identify dominant minerals in soil grains. The mineral compositions in Te hot-spots were identified to be goethite and illite (Figure S3). This suggests that Fe(III) hydroxides and illite can be the host phases of Te in soil, which is further confirmed by the distribution pattern of Te in soil obtained from the μ-XRF maps. However, Te could also be associated with amorphous (e.g., organic matter) or poorly crystalline (e.g., ferrihydrite) material that is not readily identified by XRD technique.

Tellurium μ-XANES Analyses. Tellurium K-edge μ-XANES spectra for Te hot-spots and reference materials are given in Figure 2. The peak energy of Te(VI) compound (e.g., $Na_2H_4TeO_6$ in Figure 2) was higher than that of Te(IV) (e.g., Na_2TeO_3 in Figure 2), which suggests that XANES spectrum of Te is sensitive to its chemical valence and local geometry. This distinction has been used to estimate the dominant Te speciation in solid samples.[10,18] In the soil thin section, the peak energies of hot-spots were located between that of Te(IV) and Te(VI) compounds (Figure 2), indicating that Te in contaminated soil was present as a mixture of Te(IV) and Te(VI) species.

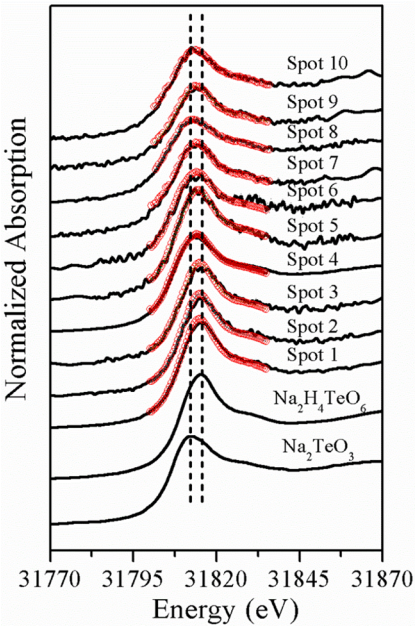

Figure 2. Te K-edge μ-XANES spectra (solid lines) of interested hot-spots in soil grains marked by open circles in Figure 1. Red dotted lines on each spectrum are simulation spectra obtained from the best LCF results by combining Na_2TeO_3 and $Na_2H_4TeO_6$ in the range of 31800−31835 eV.

The quantitative μ-XANES analysis showed that Te(VI) was the major Te species in most of hot-spots (e.g., spots 1, 2, 3, 7, 9, and 10), but pure Te(VI) or Te(IV) species cannot be found in all examined hot-spots in the soil (Table S2 and Figure 2). On average, Te(VI) and Te(IV) accounted for 61% and 39% of Te in all hot-spots, respectively (Table S2). These results suggest that Te(VI) appears to be the dominant Te species in contaminated soils from abandoned mine tailings in Kawazu Mine. This is in accordance with Eh−pH diagram for Te in Te−O−H system (Figure S4),[31,32] showing that the Te(VI) form (e.g., $HTeO_4^-$) is prevalent under neutral pH and oxic conditions, as shown for the examined soil sample. Nevertheless, microbial activities and unknown kinetics effects that cannot be considered in the simplified thermodynamic calculation can result in the transformation of Te speciation in soil. For example, Te(VI) can be stepwise reduced to Te(0) via Te(IV) under reducing conditions created by bacterial activities.[10]

Additionally, dominant Te(IV) species was also observed in some Te hot-spots (e.g., spots 4, 5, 6, and 8) in the soil thin section (Table S2 and Figure 2). Interestingly, these hot-spots (except for spot 4) contained more illite mineral than others based on their μ-XRD patterns (Figure S3), implying that Te(IV) is possibly retained by illite in the contaminated soil from waste tailings. However, goethite was the predominant mineral in almost all examined hot-spots regardless of Te species, which suggests that Fe(III) hydroxides are likely to be the host phases for both Te(VI) and Te(IV) in the contaminated soil. This finding can be supported by an earlier laboratory study concerning Te distribution in a synthetic soil-water system,[10] in which either Te(VI) or Te(IV) was shown to be strongly adsorbed by Fe(III) hydroxides in incubated soil via the formation of inner-sphere complexes.

Tellurium EXAFS Analyses. Figure 3 shows k^3-weighted $x(k)$ spectra and RSFs (phase shift not corrected) of Te K-edge EXAFS for a hot-spot (spot 4) in soil and adsorbed samples. Two small shoulders indicated by dotted lines were observed in

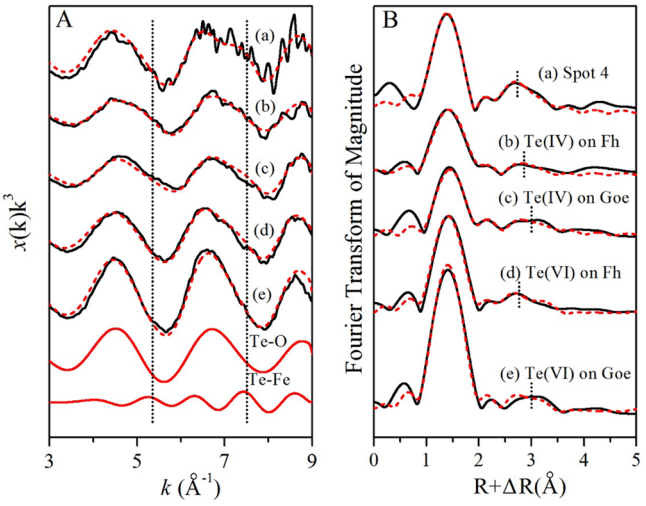

Figure 3. Te K-edge EXAFS spectra of hot-spots in soil grains and adsorbed samples: (A) k^3-weighted $x(k)$ spectra and (B) their RSFs (phase shift not corrected). Solid lines are spectra obtained by experiments, and red dashed lines are calculated spectra by curve-fitting analysis.

DOI: 10.1021/acs.est.7b00955
Environ. Sci. Technol. 2017, 51, 6027−6035

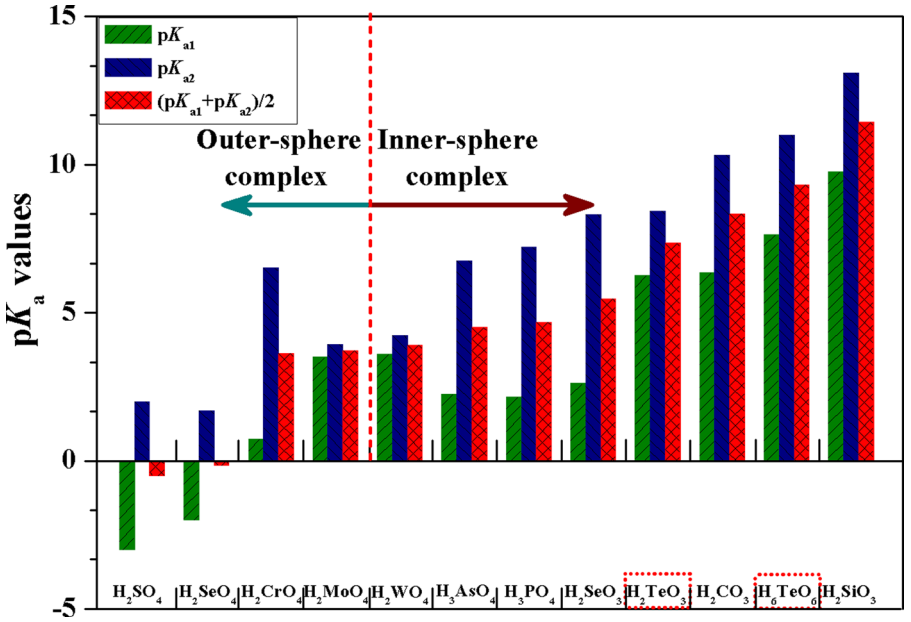

Figure 4. Relationship between pK_a values and attachment modes on ferrihydrite for various oxyanions. The pK_{a1} and pK_{a2} values are obtained from the reference.[33]

$k^3x(k)$ spectra for all samples, which were clearly overlapped by the peaks in the Te−Fe waves obtained through inverse Fourier transformation of Te−Fe shells (Figure 3A). Moreover, a prominent peak originating from Te−O bond and further distance peaks corresponding to Te−Fe shells were present in the RSFs for all samples (Figure 3B). The presences of Te−Fe shells in goethite, ferrihydrite, and spot 4 suggest that the inner-sphere complexes of Te are formed onto the surface of adsorbed samples and the Te hot-spot in the contaminated soil.

Intrinsically, the surface complex constants for oxyanions on metal oxides are dependent on proton dissociation constant pK_a of conjugate acids.[33−35] Previous studies have documented that divalent oxyanions (e.g., tungstate) prefer to form bidentate surface complexes to ferrihydrite via two oxygens from the center atom.[36,37] This means that two −OH groups of oxyanions reflected by pK_{a1} and pK_{a2} can be responsible for the stability of the surface complexes. Hence, the $p\bar{K}_a$ values, defined as $p\bar{K}_a = (pK_{a1} + pK_{a2})/2$, were proposed here to clearly predict the formation of inner-sphere or outer-sphere complexes during oxyanions adsorption on ferrihydrite. That is, conjugate anions with $p\bar{K}_a$ values larger than that of H_2WO_4 would prefer to form inner-sphere complexes onto ferrihydrite (Figure 4). In the case of $Te(IV)O_3^{2-}$ and $Te(VI)O_2(OH)_4^{2-}$, their $p\bar{K}_a$ values are higher than H_2WO_4, indicating that inner-sphere complexation would be the main attachment mode for both Te species, and the surface complex for Te(VI) could be more stable than that for Te(IV) due to larger $p\bar{K}_a$ for Te(VI). These theoretical predictions are in good agreement with above spectroscopic observations.

The structural parameters obtained by curve-fitting analyses of EXAFS data are summarized in Table S3. The first prominent shell was simulated with Te−O bond at the distance around 1.87 ± 0.01 Å and 1.89 ± 0.01 Å for Te(IV) adsorbed on ferrihydrite and goethite, respectively. While the Te−O distance for Te(VI)-adsorbed samples was 1.90 ± 0.01 Å, these values are highly comparable with earlier studies,[10,18] in which Te−O distance for Te(IV) and Te(VI) adsorbed on ferrihydrite was reported as 1.86−1.87 Å and 1.91−1.92 Å, respectively. The quantitative analysis of spot 4 in contaminated soil showed that Te−O distance in the first shell was 1.88 Å, which is between Te(IV)−O and Te(VI)−O distance obtained from adsorbed samples here and in previous studies.[10,18] This is consistent with the fact that Te in the spot 4 is present as a mixture of 67% Te(IV) and 33% Te(VI), as revealed by its μ-XANES spectrum (Figure 2 and Table S2).

The further distant shells in the RSFs for adsorbed samples were assigned as two Te−Fe shells, and the distances between Te and Fe atom were calculated as 2.92−3.10 Å (R_{Te-Fe1}) and 3.39−3.60 Å (R_{Te-Fe2}). The coordination numbers of first Te−Fe shells (CN_{Te-Fe1}) in systems of Te(IV) adsorbed on either ferrihydrite or goethite were generally less than those in Te(VI) adsorbed samples (Table S3). It has been suggested that two Te−Fe shells can be formed during Te(VI) adsorption on ferrihydrite but only one Te−Fe shell for the Te(IV) system.[18] These facts possibly indicate that the contribution from first Te−Fe shell at a distance around 3.0 Å is limited for Te(IV) adsorbed on Fe oxides, although different experimental conditions such as pH and ionic strength can affect the formation modes of surface complexes.

Moreover, the further distance peak for spot 4 in contaminated soil was also attempted to simulate by two Te−Fe shells, but the calculated distances were not strictly identical to any adsorbed samples (Table S3). This can be explained by at least two reasons: (i) the quality of μ-EXAFS spectrum for spot 4 was not so good due to possible interference from other elements in contaminated soil, although multiple scans were taken to improve signal-to-noise ratio; and (ii) model compounds could not be reasonably prepared resulting from the complicated association of Te(IV) and Te(VI) with soil grains. Nevertheless, the estimation of CNs in spot 4 showed that CN_{Te-Fe2} is much larger than CN_{Te-Fe1} (Table S3), suggesting that double corner-sharing linkage is likely to be one of preferential complexation modes for Te in soil. Because shorter interatomic distance of Te and Fe atoms possibly corresponds to edge-sharing linkage, while longer distance reflects double corner-sharing linkage.[18,38,39]

DOI: 10.1021/acs.est.7b00955
Environ. Sci. Technol. 2017, 51, 6027−6035

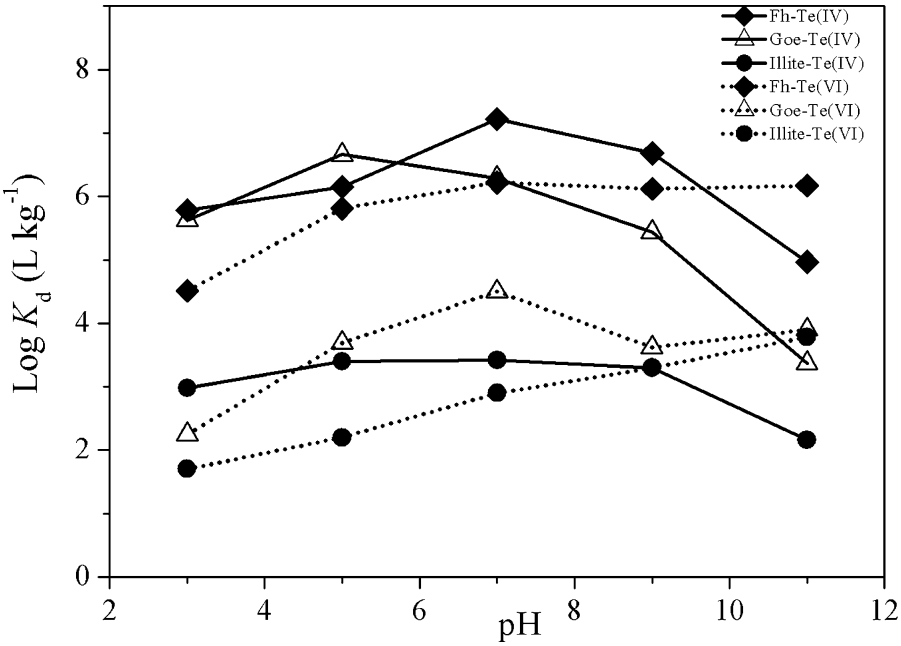

Figure 5. Adsorption envelopes for Te(IV) and Te(VI) on ferrihydrite (Fh), goethite (Goe), and illite as a function of pH. The diamond, triangle, and circle symbols represent ferrihydrite, goethite and illite, respectively. Solid and dotted lines indicate Te(IV) and Te(VI) species, respectively.

It has been highlighted that structural incorporation of Te(VI) into Fe(oxyhydr) oxide phases through co-precipitation is the main process for Te enrichment in marine ferromanganese crust.[18] However, only this mechanism cannot be sufficient to clarify the distribution and speciation of Te in soil. There are more factors affecting speciation and accumulation of Te in soil compared with the ferromanganese oxide: (i) soil has diverse Te sources such as water, atmospheric deposition, and weathering of Te-bearing rock, while seawater may be the sole source for Te in ferromanganese crusts; (ii) soil contains a variety of components such as metal oxides, clay minerals, and organic matter, whereas ferromanganese crust mainly consists of iron and manganese oxides; and (iii) the environmental conditions are significantly different in surface soil and marine ecosystem, including pH, Eh, salinity, pressure, and microorganisms, etc.

Adsorption Experiments for Te on Iron Oxides and Illite. Figure 5 presents the distribution coefficient (K_d) for Te(IV) and Te(VI) adsorbed on ferrihydrite, goethite, and illite under various pH conditions. The log K_d values obviously increased with the increase of pH under acid condition for all absorbents, while a significant decrease with increasing pH under alkaline environment was observed in all adsorption systems for Te(IV) other than Te(VI). These facts indicate that Te adsorption on iron oxides and illite is dependent on pH, which is often related to the charges loaded on the solid phase and the proton-dissociation behavior of oxyacids.[40]

Elevated log K_d values (>4.5) were found in the systems of both Te(IV) and Te(VI) adsorption on ferrihydrite and goethite under neutral pH (Figure 5), suggesting that Fe(III) hydroxides have high affinities (>98.4% of Te was adsorbed) for both Te(IV) and Te(IV) under common environmental conditions. In terms of Te species, the log K_d levels of Te(IV) were clearly greater than those of Te(VI) adsorption on ferrihydrite and goethite except for strong alkaline environments (e.g., pH = 11), implying that Te(IV) seems to be readily adsorbed by Fe oxides. Hein et al.[9] suggested that Te(IV) in seawater is preferentially scavenged by FeOOH at the surface of ferromanganese crust, which results in the fact that the thermodynamically more stable Te(IV) is less-abundant by factors of 2 to 3.5 than Te(VI) in ocean water. In addition, larger log K_d values were observed for ferrihydrite relative to goethite in either Te(IV) or Te(VI) systems, which is probably ascribed to the higher Brunauer–Emmett–Teller surface area for ferrihydrite (330 m^2 g^{-1}) than that for goethite (20 m^2 g^{-1}).[40,41] These results are consistent with the fact that Fe(III) hydroxides are the host phase of Te in solid samples demonstrated by spectroscopic methods, which is highly reasonable because oxyanions are readily adsorbed by positively charged Fe(III) hydroxides.

In contrast, lesser degree of Te adsorption was found for illite relative to iron oxides regardless of Te species and pH condition. The negatively charged illite, a 2:1 layer type clay mineral, basically exhibit three types of sorption sites: sites on the basal planar, interlayer sites, and hydroxyl groups on the sheet edges. The first and second sites exhibit negative charge, which are specifically responsible for pH-independent adsorption of cations such as cesium.[42,43] However, sorption on the hydroxyl group sites is pH-dependent because of its amphoteric nature, which is speculated to be the most relevant adsorption mechanism for anions. Recently, the complexation models involving mechanism related to surface functional groups have been successfully utilized to simulate the adsorption of Se on illite.[44,45] Furthermore, much-larger amounts of Te(IV) were adsorbed by negatively charged illite compared with Te(VI) under a relatively lower pH (Figure 5). This is likely to be partially explained because the possible species of Te(IV) such as TeO–OH$^+$ and H_2TeO_3 show some cationic properties, while Te(VI) is mainly present in the forms of anionic H_2TeO_4 and $HTeO_4^-$ under low-pH conditions (Figure S4).[31,32] These results confirm the observation that more Te(IV) was found in the hot-spots (e.g., spots 6 and 8) containing more illite in the contaminated soil from abandoned tailings by the μ-XRF–XRD–XAFS technique.

DOI: 10.1021/acs.est.7b00955
Environ. Sci. Technol. 2017, 51, 6027–6035

Comparison between Distribution and Speciation of Te and Se in Soil. For comparison with the distribution and speciation of Te, a similar data set for Se was simultaneously obtained in the soil thin section (e.g., Figure 1D, E). The distribution of Se was almost identical to that of iron according to the μ-XRF mapping data (Figure S5), as shown for Te distribution pattern in the same soil grains (Figure 1). Combining with μ-XRD results for these particles (Figure S3) suggests that Fe(III) hydroxides can be the host phases for Se and Te in the soil contaminated by waste tailings. This finding is confirmed by the fact that added Te and Se are mainly associated with Fe(III) hydroxides in incubated soil in the laboratory experiment.[10]

Selenium K-edge μ-XANES spectra for Se hot-spots were very similar to that of $NaHSeO_3$ (Figure S5), suggesting that Se(IV) is the predominant form in the contaminated soil from abandoned tailings, which is in line with the observation that Se(IV) is one of major species in soil developed on reclaimed mine lands.[46] However, a mixture of Te(VI) and Te(IV) was present in the same soil particles obtained from Te K-edge μ-XANES results (e.g., spots 7, 8, 9, and 10 in Figure 2). This significant difference in speciation of Se and Te in contaminated soil can be well explained by different structures of surface complexes for Se and Te on Fe(III) hydroxides, which has been documented by theoretical prediction and spectroscopic analysis. As shown in Figure 4, the $p\bar{K}_a$ values for conjugated anions of Se and Te present an order of Te(VI) > Te(IV) > Se(IV) > $H_2WO_4 \gg$ Se(VI), indicating that Te(VI), Te(IV), and Se(IV) prefer to form stable inner-sphere complexes on the surface of Fe(III) hydroxides, whereas Se(VI) forms less stable outer-sphere complex. These predictions have been well demonstrated by EXAFS results.[10,18,47] Thus, Se(VI) has a lower affinity to soil particles and is readily leached from soil into aquatic environment, which can be responsible for the much lesser presence of Se(VI) in the contaminated soil.

Furthermore, approximately 0.1% of Se and less than 0.001% of Te in the same soil sample were leached by water, respectively, implying that Se is much more soluble (>100 times) than Te in soil (Table S4). Similarly, the laboratory study[10] also showed that the distribution of Se to water is much higher than that of Te in the synthetic soil–water system. It has been further documented that the larger affinity of Te for soil in originates from the formation of the inner-sphere complexes of Te(IV) and Te(VI) on Fe(III) hydroxides, while higher distribution of Se to water was ascribed to highly soluble Se(VI) and its weak outer-sphere complex, as shown for dominant Se(VI) in the water phase.[10] Therefore, the difference in the speciation and solubility of Se and Te in contaminated soils from abandoned mine tailings can be strongly confirmed by the distribution behaviors of Se and Te observed in the laboratory study.

Environmental Implications. It has been suggested that numerous ions (e.g., Zn^{2+}, Cr^{3+}, Ge^{4+}, As^{5+}, and Sb^{5+}) can be structurally incorporated into Fe(III) site of iron oxides.[18,41,48,49] Compared with surface adsorption, structural incorporation cannot be greatly affected by environmental factors such as pH, ionic strength, and competitive ions, resulting in the relatively low solubility and mobility in the environment. Similarly, Te(VI) in soil can be expected to be relatively stable and difficult to mobilize if Te(VI) is structurally incorporated into Fe(III) oxides in soil as demonstrated for ferromanganese crust, although chemical processes for Te enrichment in contaminated soil could be more complicated due to various affecting factors. However, Te(IV) was also an important chemical species in addition to Te(VI) in the contaminated soil. Unlike Te(VI), Te(IV) can be adsorbed by illite and Fe(III) hydroxides in soil via the formation of surface complexes. Thus, the retention of Te(IV) in soil could be less stable than with that for Te(VI), possibly resulting in easier release and migration for Te(IV) in soil under suboxic conditions.

In the study area, the total Te concentrations in fern and moss species were 0.13 and 1.26 mg kg^{-1}, respectively. In comparison with a recent investigation,[7] these values are greatly higher than Te levels in Japanese crops ranging from 0.0001 to 0.12 mg kg-1 with a geometric mean of 0.0018 mg kg^{-1}, but the soil-to-crop transfer factors (TFs) of Te in our study are within the range of TFs in various crops (1.3×10^{-3}-2.3×10^{-1}). These facts suggest that plant uptake of Te is likely to depend on its bioavailable fraction in soil, as documented for other trace elements like Se.[50,51] It has been assumed that Te in paddy soil could be reduced to highly mobile $HTeO_3^-$ under flooded condition, resulting in higher Te concentration in brown rice than that in upland crop.[7] However, further study is necessary to clarify the bioavailability of every Te speciation in soil to different plant species.

Our study clarifies the chemical speciation and host phases of Te in the contaminated soil by the μ-XRF–XRD–XAFS techniques. These findings are of significant importance for better understanding the solubility, mobility, and bioavailability of Te in contaminated soil environments, which also can be extended to similar surface environments. As Te concentration in common samples is much lower than the level required for XAFS analysis, it is necessary to develop the modeling of solid–water distribution of Te to extend the speciation results of Te to a much-lower Te level in environment.

■ ASSOCIATED CONTENT

Supporting Information

The Supporting Information is available free of charge on the ACS Publications website at DOI: 10.1021/acs.est.7b00955.

Supplemental texts for the materials and methods section. Figures showing the location of study area, total Te concentration in soil, μ-XRD patterns of Te hot-spots, an Eh–pH diagram for Te, and the distribution and speciation of Se in contaminated soil. Tables showing the geochemical characteristics of studied samples, the best fitting results for Te K-edge μ-XANES spectra of Te hot-spots, structural parameters of EXAFS spectra for the Te hot-spot in soil and adsorbed samples, and leached results for the contaminated soil using water. (PDF)

■ AUTHOR INFORMATION

Corresponding Authors

*Phone: +86-851-85895787; fax: +86-851-85891334; e-mail: qinhaibo@vip.gyig.ac.cn.

*Phone: +81-3-5841-4517; fax: +81-3-5841-8791; e-mail: ytakaha@eps.s.u-tokyo.ac.jp.

ORCID

Hai-Bo Qin: 0000-0002-7404-3703

Notes

The authors declare no competing financial interest.

DOI: 10.1021/acs.est.7b00955
Environ. Sci. Technol. 2017, 51, 6027–6035

■ ACKNOWLEDGMENTS

This work was supported by Grants-in-Aid for Scientific Research from the Japan Society for the Promotion of Science (nos. 16K13911, 16K12627, 16H04073, 15H02149, and 24110008), the National Natural Science Foundation of China (no. 41303099), Chinese Academy of Sciences "Light of West China" Program, and State Key Laboratory of Environmental Geochemistry (no. SKLEG2015201). This study was performed with the approval of JASRI/SPring-8 (nos. 2015B0118, 2015B0127, 2016A0118, and 2016A0127) and Photon Factory (nos. 2016G632 and 2015G664).

■ REFERENCES

(1) Belzile, N.; Chen, Y. W. Tellurium in the environment: A critical review focused on natural waters, soils, sediments and airborne particles. *Appl. Geochem.* **2015**, *63*, 83−92.
(2) Ba, L. A.; Doring, M.; Jamier, V.; Jacob, C. Tellurium: an element with great biological potency and potential. *Org. Biomol. Chem.* **2010**, *8*, 4203−4216.
(3) Tang, Z. Y.; Zhang, Z. L.; Wang, Y.; Glotzer, S. C.; Kotov, N. A. Self-assembly of cdte nanocrystals into free-floating sheets. *Science* **2006**, *314*, 274−278.
(4) Deng, Z. T.; Zhang, Y.; Yue, J. C.; Tang, F. Q.; Wei, Q. Green and orange CdTe quantum dots as effective pH-sensitive fluorescent probes for dual simultaneous and independent detection of viruses. *J. Phys. Chem. B* **2007**, *111*, 12024−12031.
(5) Issa, Y. M.; Abdel-Fattah, H. M.; Shehab, O. R.; Abdel-Moniem, N. B. Determination and speciation of tellurium hazardous species in real and environmental samples. *Int. J. Electrochem. Sci.* **2016**, *11*, 7475−7498.
(6) Tagami, K.; Uchida, S.; Ishii, N.; Zheng, J. Estimation of Te-132 distribution in Fukushima Prefecture at the early stage of the Fukushima Daiichi Nuclear Power Plant reactor failures. *Environ. Sci. Technol.* **2013**, *47*, 5007−5012.
(7) Yang, G.; Zheng, J.; Tagami, K.; Uchida, S. Soil-to-crop transfer factors of tellurium. *Chemosphere* **2014**, *111*, 554−559.
(8) Cohen, B. L. Anomalous behavior of tellurium abundances. *Geochim. Cosmochim. Acta* **1984**, *48*, 203−205.
(9) Hein, J. R.; Koschinsky, A.; Halliday, A. N. Global occurrence of tellurium-rich ferromanganese crusts and a model for the enrichment of tellurium. *Geochim. Cosmochim. Acta* **2003**, *67*, 1117−1127.
(10) Harada, T.; Takahashi, Y. Origin of the difference in the distribution behavior of tellurium and selenium in a soil−water system. *Geochim. Cosmochim. Acta* **2008**, *72*, 1281−1294.
(11) Lee, D. S.; Edmond, J. M. Tellurium species in seawater. *Nature* **1985**, *313*, 782−785.
(12) Karlson, U.; Frankenberger, W. T. *Metal ions in biological systems*; Marcel Dekker: New York, 1993.
(13) Chasteen, T. G.; Fuentes, D. E.; Tantalean, J. C.; Vasquez, C. C. Tellurite: history, oxidative stress, and molecular mechanisms of resistance. *FEMS Microbiol. Rev.* **2009**, *33*, 820−832.
(14) Ramos-Ruiz, A.; Field, J. A.; Wilkening, J. V.; Sierra-Alvarez, R. Recovery of elemental tellurium nanoparticles by the reduction of tellurium oxyanions in a methanogenic microbial consortium. *Environ. Sci. Technol.* **2016**, *50*, 1492−1500.
(15) Kim, D. H.; Kim, M. G.; Jiang, S.; Lee, J. H.; Hur, H. G. Promoted reduction of tellurite and formation of extracellular tellurium nanorods by concerted reaction between iron and *Shewanella oneidensis* MR-1. *Environ. Sci. Technol.* **2013**, *47*, 8709−8715.
(16) Grundler, P. V.; Brugger, J.; Etschmann, B. E.; Helm, L.; Liu, W.; Spry, P. G.; Tian, Y.; Testemale, D.; Pring, A. Speciation of aqueous tellurium(IV) in hydrothermal solutions and vapors, and the role of oxidized tellurium species in Te transport and gold deposition. *Geochim. Cosmochim. Acta* **2013**, *120*, 298−325.
(17) Chen, Y. W.; Alzahrani, A.; Deng, T. L.; Belzile, N. Valence properties of tellurium in different chemical systems and its determination in refractory environmental samples using hydride generation-Atomic fluorescence spectroscopy. *Anal. Chim. Acta* **2016**, *905*, 42−50.
(18) Kashiwabara, T.; Oishi, Y.; Sakaguchi, A.; Sugiyama, T.; Usui, A.; Takahashi, Y. Chemical processes for the extreme enrichment of tellurium into marine ferromanganese oxides. *Geochim. Cosmochim. Acta* **2014**, *131*, 150−163.
(19) MacLean, L. C.; Beauchemin, S.; Rasmussen, P. E. Lead speciation in house dust from Canadian urban homes using EXAFS, micro-XRF, and micro-XRD. *Environ. Sci. Technol.* **2011**, *45*, 5491−5497.
(20) Mitsunobu, S.; Takahashi, Y.; Terada, Y. μ-XANES evidence for the reduction of Sb(V) to Sb(III) in soil from sb mine tailing. *Environ. Sci. Technol.* **2010**, *44*, 1281−1287.
(21) Grafe, M.; Donner, E.; Collins, R. N.; Lombi, E. Speciation of metal(loid)s in environmental samples by X-ray absorption spectroscopy: A critical review. *Anal. Chim. Acta* **2014**, *822*, 1−22.
(22) Hori, H.; Koyama, E.; Nagashima, K. Kinichilite, a new minera from the Kawazu mine, Shimoda city, Japan. *Mineral. J.* **1981**, *10*, 333−337.
(23) Shimizu, M.; Kato, A.; Matsubara, S. Hemusite and paraguanajuatite from the Kawazu mine, Shizuoka Prefecture, Japan. *Mineral. J.* **1988**, *14*, 92−100.
(24) Nakata, M.; Komuro, K. Chemistry and Occurrences of Native Tellurium from Epithermal Gold Deposits in Japan. *Resour. Geol.* **2011**, *61*, 211−223.
(25) Igarashi, N.; Nitani, H.; Takeichi, Y.; Niwa, Y.; Abe, H.; Kimura, M.; Mori, T.; Nagatani, Y.; Kosuge, T.; Kamijo, A.; Koyama, A.; Ohta, H.; Shimizu, N. Newly designed double surface bimorph mirror for BL-15A of the photon factory. *AIP Conf. Proc.* **2015**, *1741*, 040021.
(26) Zabinsky, S. I.; Rehr, J. J.; Ankudinov, A.; Albers, R. C.; Eller, M. J. Multiple-scattering calculations of X-ray-absorption spectra. *Phys. Rev. B: Condens. Matter Mater. Phys.* **1995**, *52*, 2995−3009.
(27) Jumas, J. C.; Wintenberger, M.; Philippot, E. Etude magnetique des phases du systeme $Fe_2O_3TeO_2$ structure magnetique de Fe_2TeO_5 a 4.2 K. *Mater. Res. Bull.* **1977**, *12*, 1063−1070.
(28) Krishnan, K.; Singh Mudher, K. D.; Rama Rao, G. A.; Venugopal, V. Structural and thermochemical studies on Cr_2TeO_6 and Fe_2TeO_6. *J. Alloys Compd.* **2001**, *316*, 264−268.
(29) Salminen, R.; Plant, J. A.; Reeder, S. *Geochemical atlas of Europe. Part 1, background information, methodology and maps*; Geological Survey of Finland: Espoo, Finland, 2005.
(30) Perkins, W. T. Extreme selenium and tellurium contamination in soils-an eighty year-old industrial legacy surrounding a Ni refinery in the Swansea Valley. *Sci. Total Environ.* **2011**, *412*−*413*, 162−169.
(31) Brookins, D. G. *Eh−pH diagram for geochemistry*; Springer-Verlag: Berlin, Germany, 1988.
(32) McPhail, D. C. Thermodynamic properties of aqueous tellurium species between 25 and 350°C. *Geochim. Cosmochim. Acta* **1995**, *59*, 851−866.
(33) Dzombak, D. A.; Morel, F. M. M. *Surface complexation modeling, hydrous ferric oxide*; John Wiley & Sons: New York, 1990.
(34) Dean, J. A. *Lange's Handbook of Chemistry*; 15th ed.; McGraw Hill: New York, 1999.
(35) Li, Y. H. Ultimate removal mechanisms of elements from ocean. *Geochim. Cosmochim. Acta* **1981**, *45*, 1659−1664.
(36) Kashiwabara, T.; Takahashi, Y.; Tanimizu, M.; Usui, A. Molecular-scale mechanisms of distribution and isotopic fractionation of molybdenum between seawater and ferromanganese oxides. *Geochim. Cosmochim. Acta* **2011**, *75*, 5762−5784.
(37) Kashiwabara, T.; Takahashi, Y.; Marcus, M. A.; Uruga, T.; Tanida, H.; Terada, Y.; Usui, A. Tungsten species in natural ferromanganese oxides related to its different behavior from molybdenum in oxic ocean. *Geochim. Cosmochim. Acta* **2013**, *106*, 364−378.
(38) Manceau, A.; Drits, V. A. Local structure of ferrihydrite and feroxyhite by EXAFS spectroscopy. *Clay Miner.* **1993**, *28*, 165−184.
(39) Waychunas, G. A.; Rea, B. A.; Fuller, C. C.; Davis, J. A. Surface-chemistry of ferrihydrite: part 1. EXAFS studies of the geometry of

DOI: 10.1021/acs.est.7b00955
Environ. Sci. Technol. 2017, 51, 6027−6035

coprecipitated and adsorbed arsenate. *Geochim. Cosmochim. Acta* **1993**, *57*, 2251−2269.
(40) Langmuir, D. *Aqueous environmental geochemistry*; Prentice Hall: Upper Saddle River, NJ, 1997.
(41) Mitsunobu, S.; Takahashi, Y.; Terada, Y.; Sakata, M. Antimony(V) incorporation into synthetic ferrihydrite, goethite, and natural iron oxyhydroxides. *Environ. Sci. Technol.* **2010**, *44*, 3712−3718.
(42) Qin, H. B.; Yokoyama, Y.; Fan, Q. H.; Iwatani, H.; Tanaka, K.; Sakaguchi, A.; Kanai, Y.; Zhu, J.; Onda, Y.; Takahashi, Y. Investigation of cesium adsorption on soil and sediment samples from Fukushima Prefecture by sequential extraction and EXAFS technique. *Geochem. J.* **2012**, *46*, 297−302.
(43) Fan, Q. H.; Tanaka, M.; Tanaka, K.; Sakaguchi, A.; Takahashi, Y. An EXAFS study on the effects of natural organic matter and the expandability of clay minerals on cesium adsorption and mobility. *Geochim. Cosmochim. Acta* **2014**, *135*, 49−65.
(44) Goldberg, S. Modeling selenite adsorption envelopes on oxides, clay minerals, and soils using the triple layer model. *Soil. Sci. Soc. Am. J.* **2013**, *77*, 64−71.
(45) Missana, T.; Alonso, U.; García-Gutiérrez, M. Experimental study and modelling of selenite sorption onto Illite and smectite clays. *J. Colloid Interface Sci.* **2009**, *334*, 132−138.
(46) Ryser, A. L.; Strawn, D. G.; Marcus, M. A.; Fakra, S.; Johnson-Maynard, J. L.; Möller, G. Microscopically focused synchrotron X-ray investigation of selenium speciation in soils developing on reclaimed mine lands. *Environ. Sci. Technol.* **2006**, *40*, 462−467.
(47) Hayes, K. F.; Roe, A. L.; Brown, G. E.; Hodgson, K. O.; Leckie, J. O.; Parks, G. A. In situ x-ray absorption study of surface complexes: selenium oxyanions on a-FeOOH. *Science* **1987**, *238*, 783−786.
(48) Manceau, A.; Schlegel, M. L.; Musso, M.; Sole, V. A.; Gauthier, C.; Petit, P. E.; Trolard, F. Crystal chemistry of trace elements in natural and synthetic goethite. *Geochim. Cosmochim. Acta* **2000**, *64*, 3643−3661.
(49) Martinez, C. E.; McBride, M. B. Cd, Cu, Pb, and Zn coprecipitates in Fe oxides formed at different pH: aging effects on metal solubility and extractability by citrate. *Environ. Toxicol. Chem.* **2001**, *20*, 122−126.
(50) Qin, H. B.; Zhu, J. M.; Su, H. Selenium fractions in organic matter from Se-rich soils and weathered stone coal in selenosis areas of China. *Chemosphere* **2012**, *86*, 626−633.
(51) Qin, H. B.; Zhu, J. M.; Liang, L.; Wang, M. S.; Su, H. The bioavailability of selenium and risk assessment for human selenium poisoning in high-Se areas, China. *Environ. Int.* **2013**, *52*, 66−74.

DOI: 10.1021/acs.est.7b00955
Environ. Sci. Technol. 2017, 51, 6027−6035